

Formation and termination of runaway beams during vertical displacement events in tokamak disruptions

J.R.Martín-Solís^{1a}, J.A. Mier², M. Lehnen³, and A. Loarte³

¹*Universidad Carlos III de Madrid, Avenida de la Universidad 30, 28911-Madrid, Spain*

³*Universidad de Cantabria, Avenida de los Castros s/n, 39005, Santander, Spain*

³*ITER Organization, Route de Vinon sur Verdon, 13115 St Paul Lez Durance, France*

Abstract.

A simple 0-D model which mimics the plasma surrounded by the conducting structures [D.I. Kiramov, B.N. Breizman, *Physics of Plasmas* **24**, 100702 (2017)] and including self-consistently the vertical plasma motion and the generation of runaway electrons during the disruption is used for an assessment of the effect of vertical displacement events on the runaway current formation and termination. The total plasma current and runaway current at the time the plasma hits the wall is estimated and the effect of injecting impurities into the plasma is evaluated. In the case of ITER, with a highly conducting wall, although the total plasma current when the plasma touches the wall is the same for any number of injected impurities, however the fraction of the plasma current carried by runaway electrons can significantly decrease for large enough amounts of impurities. The plasma velocity is larger and the time when the plasma hits the wall shorter for lower runaway currents, which are obtained when larger amounts of impurities are injected. When the plasma reaches the wall, the scraping-off of the runaway beam occurs and the current is terminated. During this phase, the plasma vertical displacement velocity and electric field can substantially increase leading to the deposition of a noticeable amount of energy on the runaway electrons (\sim hundreds of MJ). It is found that an early second impurity injection reduces somewhat the amount of energy deposited by the runaways.

Also larger temperatures of the companion plasma during the scraping-off might be efficient in reducing the power fluxes due to the runaways onto the PFCs. The plasma reaches the $q_a = 2$ limit before the runaway electron current is terminated and by that time the amount of energy deposited on the runaway electrons can be substantially lower than that expected until the beam is fully terminated. Negligible additional conversion of magnetic into runaway kinetic energy is predicted during the runaway deconfinement following the large magnetic fluctuations after $q_a = 2$ is crossed for characteristic deconfinement times lower than 0.1 ms which is a characteristic timescale for ideal MHD instabilities to develop.

PACS numbers: 52.55.Fa, 52.27.Ny, 52.50.-b

^{a)} *electronic-mail: solis@fis.uc3m.es*

1 INTRODUCTION

Large amounts of runaway electrons are predicted during ITER disruptions which could lead to severe damage (erosion and melting) and limit the lifetime of the plasma facing components (PFCs) [1]. Indeed, the control and mitigation of the runaway electrons constitute one of the priorities of the disruption mitigation system (DMS) in ITER [2], the injection of high-Z impurities by Shattered Pellet Injection (SPI) actually constituting the most promising candidate.

Modelling and evaluation of the runaway current formation during the disruption has been often carried out without including self-consistently the vertical motion of the plasma [3] which often occurs during the disruptive event [4]. During the current quench phase of the disruption, the plasma current decays and runaway electrons are generated, replacing the plasma current and, at the same time, the plasma moves vertically until it finally hits the wall. Then, the scraping-off of the plasma column starts leading to the deposition of the runaway energy onto the PFCs, which can noticeably increase due to the conversion of magnetic into runaway kinetic energy, as has been extensively studied in the past [6, 7, 8, 9, 10, 11]. Moreover, it has been predicted that mitigation of disruptions by injection of a large amount of impurities can accelerate the vertical plasma motion which, when the scraping-off of the beam happens, can largely increase the amount of energy deposited by the runaway electrons [7].

Here, a simple 0-D model which mimics the plasma surrounded by the conducting structures [12], including self-consistently the vertical plasma motion and the generation of runaway electrons during the disruption, will be used for an evaluation of the effect of vertical displacement events on the formation of the runaway current and its termination (scraping-off) during the disruption. Despite being simple, the 0-D model is able to

capture the physics essential to the problem, including in some cases analytical approximations, and allows an easier and faster identification of the dominant processes and essential parameters, while requiring less detailed knowledge of density, temperature and current density profiles during the current quench which are poorly known. The basics of the model [12] are reviewed in Sec. 2, whereas the consequences for the formation and termination of the runaway beam constitute the subject of Secs. 3 and 4, respectively. The conclusions are summarized in Sec. 6.

2 THE THREE-LOOP MODEL

The model here used is based on Ref. [12, 13] and approximates the plasma-wall system by a set of three parallel thin circular coaxial rings of radius R_0 . The bottom and top conductors carry currents I_1 , I_2 , respectively, and represent the current in the conducting wall, while the middle conductor represents the plasma current, I_p , which can move vertically. The three-loop model also includes a static external magnetic field created by two constant circular currents, I_e . Their current I_e does not change, which mimics shielding of the additional loops by the first wall. The corresponding circuit equations are [12]:

$$L_w \frac{dI_1}{dt} + L_{12} \frac{dI_2}{dt} + L_{wp} \frac{d}{dt} [1 - \kappa \ln(1 + \xi)] I_p = -R_w I_1, \quad (1)$$

$$L_{12} \frac{dI_1}{dt} + L_w \frac{dI_2}{dt} + L_{wp} \frac{d}{dt} [1 - \kappa \ln(1 - \xi)] I_p = -R_w I_2, \quad (2)$$

$$L_{wp} \frac{d}{dt} [1 - \kappa \ln(1 + \xi)] (I_1 + I_e) + L_{wp} \frac{d}{dt} [1 - \kappa \ln(1 - \xi)] (I_2 + I_e) + \frac{d(L_p I_p)}{dt} = -R_p (I_p - I_r) \quad (3)$$

where I_r is the runaway current (note that $I_p = I_r + I_{OH}$, where I_{OH} is the ohmic or

resistive current), $\xi \equiv z/a_w$ is the normalized vertical displacement of the plasma ($2a_w$ is the distance between the two wall conductors), $\kappa = (\ln [8R_0/a_w] - 2)^{-1}$, and all the resistance and inductance coefficients are defined in [12]: R_w and L_w are the resistance and inductance of the wall conductors, respectively, L_{12} is the mutual inductance between the wall conductors, and the mutual inductances of the plasma and the wall conductors are $L_{1p} = L_{wp} [1 - \kappa \ln(1 + \xi)]$, $L_{2p} = L_{wp} [1 - \kappa \ln(1 - \xi)]$, respectively; L_p is the total plasma inductance, $L_p \equiv L_{int} + L_{ext}$, where L_{int} and L_{ext} are the internal and external plasma inductances, respectively, with $L_{ext} \equiv \mu_0 R_0 (\ln (8R_0/a) - 2)$, and R_p is the plasma resistance, $R_p \approx \eta 2R_0/a^2$ (η is the plasma resistivity and a the plasma minor radius).

The force free-constraint

$$\xi = \frac{I_1 - I_2}{I_1 + I_2 + 2I_e}, \quad (4)$$

is used for the vertical plasma motion [12].

The model also includes an equation for the runaway current

$$\frac{dI_r}{dt} = \left(\frac{dI_r}{dt} \right)_{seed} + \left(\frac{dI_r}{dt} \right)_{avalanche}. \quad (5)$$

The first term in Eq. (5) corresponds to the generation of the runaway seed current (which can include different mechanisms such as the Dreicer [14, 15] process, the hot tail runaway electron generation mechanism [16], tritium decay or Compton scattering of γ rays emitted by the activated wall in the case of DT plasmas [3]). The second term describes the avalanche runaway generation, approximated by [17]

$$\left(\frac{dI_r}{dt} \right)_{avalanche} \approx \frac{e (E_{||} - E_R) I_r}{m_e c \ln a(Z)}. \quad (6)$$

Here, $a(Z) \equiv \sqrt{3(5+Z)/\pi}$, $E_R = n_e e^3 \ln \Lambda / 4\pi \epsilon_0^2 m_e c^2$ is the critical field for runaway generation [15, 18], and the parallel electric field, $E_{||}$, is determined taking into account

the replacement of the plasma current by the runaway current,

$$E_{||} = \eta(j_p - j_r), \quad (7)$$

where $j_{p,r} = I_{p,r}/\pi a^2 k$ and k is the plasma elongation. For simplicity, runaway losses will be neglected during the current quench phase of the disruption, until the scraping-off of the beam starts when the plasma touches the wall. Also, as in Ref. [17], we will assume *ad-hoc* constant values for $\ln\Lambda$ (typically $\sim 10 - 17$) and Z . In fully ionized plasmas, Z is the effective ion charge, whereas in disruptive plasmas with impurities, Z includes the effect of the scattering of the runaway electrons on the impurity ions and atomic nuclei. In that case the expression for the avalanche amplification must be generalized to include the effect of the collisions with the bound electrons [20, 21, 22, 23].

3 RUNAWAY FORMATION

During the current quench phase of the disruption, the plasma current decays and runaway electrons are generated.

Our modeling starts just after the thermal quench, assuming an initial primary runaway seed $I_{seed} = I_r(t = 0)$. Then, according to Eq. (6), the runaway current at each time can be written

$$I_r(t) = I_{seed} \exp\left(\int_0^t \frac{ec(E_{||} - E_R)}{T_r} dt'\right), \quad (8)$$

with $T_r \equiv m_e c^2 \ln\Lambda a(Z)$, and the plasma current at each time during the vertical motion can be obtained solving the equations (1) - (3) for the inductively coupled circuits and taking into account the force-free condition (4) for the vertical displacement.

Full line in Fig. 1 shows the numerically calculated plasma current at the time the plasma hits wall as a function of the ratio of the current quench time ($\tau_{CQ} \sim L_{int}/R_p$) to the wall time ($\tau_w \equiv L_w/R_w$) for a 15 MA ITER-like disruption, assuming a runaway seed $I_{seed} = 0.03$ MA and $n_e = 4 \times 10^{21} \text{ m}^{-3}$. Note that, when $\tau_{CQ} \ll \tau_w$ (the case of a perfectly conducting wall) no external magnetic energy penetrates into the plasma and the plasma current when the plasma hits the wall tends to a constant limiting value. In contrast, when $\tau_{CQ} > \tau_w$, penetration of external magnetic energy leads to an increase of the plasma current at wall contact. Note that for sufficiently large τ_{CQ}/τ_w the plasma current at the time of wall contact might exceed 15 MA, corresponding to τ_{CQ} in excess of 50 s which is unphysical for ITER.

The vertical velocity during the plasma motion can be estimated from the equation for the plasma current. Hence, from Eq. (3), the electric field can be written

$$E_{\parallel} = \frac{I_{OH}R_p}{2\pi R_0} = -\frac{1}{2\pi R_0} \frac{dF}{dt} \quad (9)$$

where $I_{OH} = I_p - I_r$ is the ohmic current, and F is the magnetic flux across the circular contour of the plasma current,

$$F = L_{wp} [1 - \kappa \ln(1 + \xi)] (I_1 + I_e) + L_{wp} [1 - \kappa \ln(1 - \xi)] (I_1 + I_e) + L_p I_p, \quad (10)$$

and so

$$E_{\parallel} = -\frac{1}{2\pi R_0} \frac{dF}{dt} = -\frac{1}{2\pi R_0} \frac{dF}{dz} v_p \implies v_p = -2\pi R_0 \frac{E_{\parallel}}{(dF/dz)} = -\frac{R_p(I_p - I_r)}{(dF/dz)}. \quad (11)$$

Then, the time to hit the wall would be given by

$$\tau = - \int_{z_0}^{z_c} \frac{(dF/dz)}{R_p(I_p - I_r)} dz \quad (12)$$

(z_0 : initial vertical position; z_c : vertical position when contacting the wall).

These results indicate that the vertical plasma velocity must be larger (and hence the time to reach the wall shorter) for low runaway currents and viceversa, the plasma velocity must be lower (and the time to reach the wall larger) for large amounts of runaway electrons (note that our model is 0-D and does not account for possible changes to the current profile depending on the proportion of runaway electrons which can have a second order effect on the speed of the plasma movement). As a result, if a large runaway production occurs before the plasma touches the wall, the plasma velocity might be so small and the time to hit the wall increase so much that a large penetration of external magnetic energy can occur, leading to an effective current quench time larger than its nominal value, τ_{CQ} , and increasing the value of the current when the plasma touches the wall. This is illustrated by the dashed line in Fig. 1 which shows the plasma current at the time the plasma hits the wall as a function of τ_{CQ}/τ_w for a lower density, $n_e = 2.5 \times 10^{20} \text{ m}^{-3}$. The case of lower density (dashed line) leads to larger runaway production and hence to a slower plasma motion and a longer time to reach the wall which explains the larger value of the plasma current when hitting the wall for $\tau_{CQ}/\tau_w \ll 1$ due to the penetration of external magnetic energy. When the density is sufficiently increased (for densities larger than $\sim 3 \times 10^{21} \text{ m}^{-3}$ in this example), due to the reduction of the runaway current, the motion of the plasma is fast enough so that the penetration of external magnetic energy is not playing a role for $\tau_{CQ}/\tau_w \ll 1$ and the current at the wall approaches to the full line curve. This is the limit of a *highly conducting wall*.

In this work, from now on, we will be interested in the case of disruptions mitigated by impurity injection, for which the density is large enough so that in the case of ITER ($\tau_{CQ} \ll \tau_w$) the limit of a highly conducting wall can be applied. This limit was discussed in Ref. [12] and allows to get some analytical results. Hence, following [12], assuming

$R_w \rightarrow 0$, from Eqs. (1) and (2), the plasma current as a function of the normalized vertical displacement, $\xi \equiv z/a_w$, can be obtained, yielding

$$I_p(\xi) = \frac{c_2 - 2I_e \xi (L_w - L_{12}) - L \xi c_1}{L_{wp} (l_1(\xi) - L \xi l_2(\xi))}, \quad (13)$$

with

$$L \equiv \frac{L_w - L_{12}}{L_w + L_{12}}; \quad l_1(\xi) \equiv \kappa \ln \frac{1 - \xi}{1 + \xi}; \quad l_2(\xi) \equiv 2 - \kappa \ln(1 - \xi^2), \quad (14)$$

and c_1, c_2 constants given by the initial conditions [12],

$$c_1 \approx 2L_{wp}I_p(0); \quad c_2 \approx 2\xi(0) \{I_e (L_w - L_{12}) - \kappa L_{wp} I_p(0)\}. \quad (15)$$

Eq. (13) shows a monotonic dependence of I_p on the vertical displacement, ξ . It also implies that the plasma should always hit the wall at the same current, I_p .

For the currents I_1, I_2 at the wall conductors, assuming again $R_w \rightarrow 0$, it is obtained:

$$I_1 = \frac{q + p}{2}; \quad I_2 = \frac{q - p}{2} \quad (16)$$

with

$$q \equiv \frac{c_1 - L_{wp} [2 - \kappa \ln(1 - \xi^2)] I_p}{L_w + L_{12}}; \quad p \equiv \frac{c_2 - L_{wp} \kappa \ln \left[\frac{1 - \xi}{1 + \xi} \right] I_p}{L_w - L_{12}}. \quad (17)$$

From Eq. (11), in the limit of a highly conducting wall, the plasma velocity can be written straightforwardly in terms of the normalized vertical displacement as

$$v_p(\xi) = -2\pi R_0 a_w \frac{E_{||}}{(dF/d\xi)} = -\frac{a_w R_p (I_p(\xi) - I_r(\xi))}{(dF/d\xi)}, \quad (18)$$

and the corresponding time to reach a given vertical position, ξ ,

$$\tau(\xi) = - \int_{\xi_0}^{\xi} \frac{(dF/d\xi)}{R_p (I_p(\xi) - I_r(\xi))} d\xi. \quad (19)$$

We can consider now, for a given runaway seed current, $I_{seed} \equiv I_r(t=0)$, the amount of runaway electrons that can be expected to be generated during the disruption current quench due the avalanche mechanism as a function of the plasma vertical displacement. In order to simplify the analysis, we first neglect the collisional dissipation of the runaway beam ($E_{\parallel} \gg E_R$). Thus, from Eq. (8),

$$I_r \approx I_{seed} \exp\left(\int_0^t \frac{ec E_{\parallel}}{T_r} dt'\right), \quad (20)$$

and taking into account that $E_{\parallel} = -(1/2\pi R_0) dF/dt$, it is straightforward to obtain

$$I_r \approx I_{seed} e^{G_{av}(\xi)}, \quad (21)$$

where

$$G_{av}(\xi) \equiv \frac{ec(F_0 - F(\xi))}{2\pi R_0 T_r}, \quad (22)$$

is the avalanche gain at ξ , determined by the change in the magnetic flux, $F(\xi)$, given by (10) (F_0 is the value of the magnetic flux after the thermal quench).

If the collisional dissipation, E_R , cannot be neglected Eq. (21) must be generalized to

$$I_r \approx I_{seed} e^{G_{av}(\xi)} e^{-\frac{ec}{T_r} E_R \tau(\xi)} = I_{seed} e^{\frac{ec(F_0 - F(\xi))}{2\pi R_0 T_r}} e^{\frac{ec E_R}{T_r} \int_{\xi_0}^{\xi} \frac{(dF/d\xi)}{R_p(I_p(\xi) - I_r(\xi))} d\xi}, \quad (23)$$

where Eq. (19) for $\tau(\xi)$ has been used.

Taking logarithms on both sides of (23) and then taking the derivative with respect to ξ , the calculation of $I_r(\xi)$ can be reduced to the first order differential equation

$$I_r' + \left(\frac{ecF'}{2\pi R_0 T_r}\right) I_r = -\frac{ec E_R}{T_r} \frac{F'}{R_p} + \frac{ec E_R}{T_r} \frac{F'}{R_p} \frac{I_p}{I_p - I_r}. \quad (24)$$

Fig. 2 shows the numerically calculated plasma and runaway currents when the plasma hits the wall as function of n_e for a 15 MA ITER disruption ($\tau_w = 0.5$ s) and

$I_{seed} = 0.03 \text{ MA}$. The plasma touches the wall always at the same current ($\sim 9 \text{ MA}$ in this case), whereas the runaway current decreases, approximately in an exponential way, with n_e ($I_r \sim \exp(-(ec/T_r) E_R \tau)$, and $E_R \propto n_e$). The vertical plasma velocity when the beam touches the wall, as illustrated in Fig. 3, increases with density due to the decrease of the runaway current with n_e , indicating the acceleration of the VDE for larger amounts of impurities.

4 SCRAPING-OFF AND CURRENT TERMINATION

When the runaway beam touches the wall, the scraping-off phase starts, during which the plasma radius is progressively reduced, and the runaway energy is deposited onto the wall. The effect of the scraping-off of the beam, for $\xi_c < \xi < 1$ (ξ_c is the normalized vertical position of beam at the contact point, $\xi_c \equiv z_c/a_w$), can be modelled using again the equations (1) - (3) for the inductively coupled circuits, together with the force-free condition (4), and including in the equation for the runaway current a loss term $dI_r/dt \approx 2\dot{a} I_r/a$ [24], so that,

$$\frac{dI_r}{dt} \approx \frac{ec(E_{||} - E_R)}{T_r} I_r + \frac{2\dot{a}}{a} I_r \quad (25)$$

(note that during the scraping-off phase, $\xi = (a_w - a(t))/a_w = 1 - a(t)/a_w$).

According to (25), the scraping-off of the beam leads to a radial loss of the runaway current which can be described by a characteristic loss time, $\tau_d \approx a/2\dot{a}$ and, as a result, the formation of the runaway current during scraping-off takes place under an effective critical field for the generation of the runaway current enhanced by the radial losses [29],

$E_R^{eff} = E_R + T_r/ec\tau_d$, so that $dI_r/dt \propto (E_{||} - E_R^{eff})$. If $E_{||} > E_R^{eff}$, runaway current can be generated by avalanche whereas, when $E_{||} < E_R^{eff}$, runaway current is lost and the termination of the runaway current takes place.

Eq. (25) can be solved to yield the runaway current during the scraping-off phase,

$$I_r = I_{r0} \left(\frac{a}{a_0} \right)^2 \exp \left(\int_{t_c}^t \frac{ec(E_{||} - E_R)}{T_r} dt' \right), \quad (26)$$

where I_{r0} is the runaway current when the plasma touches the wall, a_0 the plasma minor radius at that time, and t_c is the time at which the beam hits the wall. And using $E_{||} = -(1/2\pi R_0) dF/dt$,

$$\begin{aligned} I_r &= I_{r0} \left(\frac{a}{a_0} \right)^2 \exp \left(\frac{ec(F_c - F(\xi))}{2\pi R_0 T_r} \right) \exp \left(-\frac{ec}{T_r} E_R \tau(\xi) \right) \\ &= I_{r0} \left(\frac{1 - \xi}{1 - \xi_c} \right)^2 \exp \left(\frac{ec(F_c - F(\xi))}{2\pi R_0 T_r} \right) \exp \left(-\frac{ec}{T_r} E_R \tau(\xi) \right). \end{aligned} \quad (27)$$

Here, the relation $a = a_w (1 - \xi)$ for the plasma minor radius as a function of the normalized vertical displacement during the scraping-off phase has been used, $F(\xi)$ is the magnetic flux for the vertical displacement ξ , given by Eq. (10), F_c the magnetic flux at the time the beam hits the wall, and

$$\tau(\xi) = - \int_{\xi_c}^{\xi} \frac{(dF/d\xi)}{R_p(I_p(\xi) - I_r(\xi))} d\xi.$$

In the case of a perfectly conducting wall, the currents $I_p(\xi)$, $I_1(\xi)$, $I_2(\xi)$, are given by Eqs. (13) - (17), and $I_r(\xi)$ during the scraping-off phase and termination, taking logarithms on both sides of (27) and then differentiating with respect to ξ , is determined by the solution of the first order differential equation

$$I_r' + \left(\frac{2}{1 - \xi} + \frac{ecF'}{2\pi R_0 T_r} \right) I_r = -\frac{ec E_R F'}{T_r R_p} + \frac{ec E_R F'}{T_r R_p} \frac{I_p}{I_p - I_r}. \quad (28)$$

Fig. 4 (top) shows as example the numerically calculated plasma current and runaway current as a function of time for a 15 MA ITER-like disruption ($\tau_w = 0.5$ s, $T_e = 5$ eV), assuming $I_{seed} = 0.03$ MA and $n_e = 10^{22}$ m⁻³. The plasma touches the wall at ~ 9 ms, indicated by the first vertical line, and the scraping-off phase starts. Note that initially, during the scraping-off phase the runaway current increases, until at a certain time, indicated by the second vertical line, the runaway current starts to decay. This can be better understood with the aid of the bottom figure which shows the time evolution of the electric field (full line). The dashed line in the figure indicates the calculated effective critical field, E_R^{eff} , and the red horizontal line the avalanche threshold, E_R . During the whole scraping-off phase, the electric field remains larger than E_R . Initially, $E_{||} > E_R^{eff}$, leading to runaway current generation and, once $E_{||} < E_R^{eff}$ the runaway current decays. Note that the runaway decay phase follows a marginal stability scenario determined by E_R^{eff} [29], during which the electric field remains close (but below) to E_R^{eff} , so that also during the runaway current decay the electric field is larger than E_R (as $E_R^{eff} = E_R + T_r/ec\tau_d > E_R$). This, as a consequence, results in a substantial energy deposition onto the runaway population, proportional to $(E_{||} - E_R)$, and conversion of magnetic into runaway kinetic energy [29].

The energy transferred to the runaway electrons as a function of time can be calculated

$$\Delta W_{run} \approx 2\pi R_0 \int_0^t I_r (E_{||} - E_R) dt' = 2\pi R_0 I_{r0} \int_0^t (E_{||} - E_R) \left(\frac{a}{a_0}\right)^2 e^{\frac{\int_0^{t'} ec(E_{||} - E_R) dt''}{T_r}} dt', \quad (29)$$

which, integrating by parts and using (26), yields

$$\Delta W_{run} \approx \frac{2\pi R_0 T_r}{ec} \left\{ (I_r - I_{r0}) - 2 \int_0^t \frac{I_r}{a} da \right\} = \frac{2\pi R_0 T_r}{ec} \left\{ (I_r - I_{r0}) + 2 \int_{\xi_c}^{\xi} \frac{I_r}{1 - \xi'} d\xi' \right\}. \quad (30)$$

The calculated energy deposition onto the runaway electrons, ΔW_{run} , as a function of time is shown in Fig. 5 (the figure also includes the energy deposited during the formation phase $\sim 2\pi R_0 T_r I_r/ec$). The total amount of energy deposited onto the runaways is larger than 100 MJ.

The results for a case with the same parameters but a larger density, $n_e = 5 \times 10^{22} \text{ m}^{-3}$, are presented in Figs. 6 and 7. It is found that although the larger density results in a noticeable reduction of the runaway current during the formation phase, the electric field during scraping-off, proportional to the plasma velocity (and so larger because of the lower runaway current), is substantially enhanced, which yields a large increase in the runaway current and substantial energy deposition during the scraping-off and the termination of the runaway current.

This is better illustrated in Fig. 8, which shows for the same disruption conditions than previous figures, the energy deposited on the runaway electrons during the scraping-off phase as a function of density. A density $n_e = 5 \times 10^{21} \text{ m}^{-3}$ is assumed at the start of the current quench, increasing to n_e due to a second impurity injection at Δt . Even if the density increase has a large impact on the magnitude of the runaway current until the beam touches the wall (Fig. 2), the large electric field induced during scraping-off compensates to large extent the effect of the density increase, which results only in a slight decrease of ΔW_{run} when n_e increases. It is also observed that an earlier second impurity injection (smaller Δt) favors somewhat a reduction in the amount of energy deposited on the runaways. Finally, these results are also found to be strongly sensitive to the assumed temperature during scraping-off, larger temperatures leading to larger induced ohmic currents and so being efficient in reducing the power fluxes onto PFCs (white squares in the figure).

However, it is not physically correct to assume that the conversion of magnetic into runaway kinetic energy lasts until the beam is fully scraped-off since, due to the decrease of the beam radius, the limit $q_a = q(r = a) = 2$ will be reached before, as illustrated in Fig. 9. It is therefore an important question if additional substantial conversion of magnetic into runaway energy may occur when the $q_a = 2$ stability boundary is crossed, or as suggested in [25, 26], the global nature of the deconfinement of the runaways by large magnetic fluctuations, δB , when $q_a = 2$ is reached can give rise to significantly larger wetted areas and conversion of magnetic to kinetic energy of the runaway electrons may be avoided when they are deconfined by large magnetic fluctuations. As shown in Fig. 10, the amount of energy deposited on the runaway electrons by the time the limit $q_a = 2$ is reached can be noticeably lower than the values estimated for the full scraping-off of the beam (Fig. 8). This result is also illustrated by Figs. 11 and 12 which show for the same conditions than Fig. 10 the runaway current and $I_r/(1 - \xi)$ [whose integration determines the energy deposited on the PFCs as indicated by Eq. (30)] as a function of the (normalized) vertical displacement, ξ , for different values of the density. The figures show that, both, the runaway current and $I_r/(1 - \xi)$ substantially decrease for increasing values of n_e until $q_a = 2$ (indicated by the second vertical line) but, later on, due to the increasing plasma velocity and enhanced electric field, both of them strongly increase reaching similar values for all densities, which explains why the total energy deposited on the runaways until the beam is fully scraped-off decreases much more slowly with increasing plasma density.

In order to evaluate the effect of the runaway deconfinement when $q_a = 2$ is crossed, a loss term $-I_r/\tau_d$ has been added to the equation for the runaway current, where τ_d is a characteristic time describing the deconfinement of the runaway electrons when the

limit $q_a = 2$ is reached. In Ref. [10] it was shown that for short enough deconfinement times, below 1 ms, the amount of energy deposited on the runaway electrons for ITER-like conditions would be noticeably reduced. However, such analysis did not consider the vertical displacement of the beam which, as illustrated in Fig. 13 for an example assuming $n_e = 10^{22} \text{ m}^{-3}$, $T_e = 5 \text{ eV}$ and $\tau_d = 0.25 \text{ ms}$, can greatly increase the energy deposited on the runaway population. The top figure shows the time evolution of the plasma current (full line), ohmic current (dashed line) and runaway current (dashed dot line), the electric field during deconfinement is presented in the middle figure, and the bottom figure shows the energy deposited on the runaway electrons. The runaway current initially decreases but the plasma current decays before the runaway current is terminated so that the plasma moves and the electric field increases due to the plasma motion (the electric field is not anymore proportional to the ohmic current because of the increase in the plasma resistance when the plasma radius is reduced). Such increase in the electric field yields substantial runaway avalanche which eventually leads to the recovery of the runaway current and to a large energy deposition on the runaway electrons (more than 100 MJ). We note that some of the features of our simple modelling can lead to a higher rate of magnetic to runaway kinetic energy conversion than would happen in the real disruptive plasma conditions in ITER. For example the 3-conductor model that we have used allows for higher penetration of external magnetic energy, which can eventually convert to runaway kinetic energy during the current quench than the previous co-axial model for the vacuum vessel with a static single wire plasma [10]. To reduce the conversion of magnetic into runaway kinetic energy to low enough values demands shorter deconfinement times, close or below 0.1 ms, as in the example presented in Fig. 14, for which $n_e = 10^{22} \text{ m}^{-3}$, $T_e = 5 \text{ eV}$ and $\tau_d = 0.1 \text{ ms}$. In this case, the decay of the runaway current is so fast that I_r is terminated before the plasma current can change and the

plasma moves, so that during runaway termination there is no increase of the electric field due to the plasma motion and the energy deposited on the runaways is kept small (~ 3 MJ). The enhancement of the electric field due to the plasma motion occurs later when there are no runaways in the plasma.

If the losses are assumed to be due to large magnetohydrodynamic instabilities, an estimate of the associated fluctuation level might be obtained using $\tau_d \sim a^2/j_0^2 D_r$ where j_0 is the first zero of the Bessel function J_0 , and D_r the radial diffusion coefficient describing the runaway losses in the stochastic magnetic field which, assuming free streaming along the field lines, could be estimated $D_r = D_m v_{\parallel}$ [27], where v_{\parallel} is the parallel electron velocity and D_m is the magnetic line diffusion coefficient $D_m = L_{\parallel} \tilde{b}^2$ (\tilde{b} is the normalized radial magnetic fluctuation amplitude $\tilde{b} \equiv \tilde{B}_r/B_0$, $L_{\parallel} \approx \pi q_0 R_0$ is the parallel correlation length of the magnetic fluctuations, and $q_0 = 2$ the safety factor), yielding for $\tau_d < 0.1$ ms a magnetic fluctuation level $\tilde{b} > 6 \times 10^{-4}$. Note that timescales < 0.1 ms are typical for ideal MHD instabilities leading to sudden confinement losses during disruptions [28].

5 RUNAWAY HEAT LOADS

The analysis carried out in the previous section has shown that substantial conversion of magnetic energy into runaway kinetic energy might be expected during the scraping-off phase of disruptions in ITER, unless the density is sufficiently large and short enough deconfinement times are assumed after $q_a = 2$ is reached. Nevertheless, for an assessment of the possible consequences for the PFCs, not only the magnitude of the deposited energy but also the timescale of the energy deposition should be considered. Hence, Fig. 15 shows for the same cases than Figs. 5 and 7, as a function of time, the energy deposited

by the runaway electrons onto the PFCs, W_{PFC} , determined by the difference between the total energy deposited on the runaways, ΔW_{run} , calculated in the previous section, minus the instantaneous kinetic energy of the runaway beam, $W_{kin} \approx 2\pi R_0 T_r I_r / ec$ [29], also shown in the figure (dashed lines), so that $W_{PFC} \equiv \Delta W_{run} - W_{kin}$ (full lines). Note that the energy deposited on the PFCs, W_{PFC} , is determined by the second term in Eq. (30).

The resulting power loads due to the deposition of runaways, $P_r(t) \equiv dW_{PFC}/dt$ (energy deposited by the runaways/time), are illustrated in Fig. 16. The vertical dashed lines indicate the time at which the limit $q_a = 2$ is reached. As observed in the figure, at larger densities, due to the faster motion of the plasma and the resulting enhancement of the induced electric field, the runaway power loads increase but the PFCs are exposed to this power flux for a shorter timescale which explains the decrease in the total amount of energy deposited when the density increases.

As it was explained in Ref. [10], a simple estimate of the increase in the surface temperature of the PFCs due to the runaway heat loads can be obtained from the solution of the one-dimensional heat diffusion equation in a semi-infinite solid [30, 10]. Hence, assuming an exponential decay of the runaway electron energy deposition into the PFCs, the surface temperature increase can be estimated [31, 32, 10]:

$$\Delta T = \frac{\kappa}{K\delta} \int_0^t q_r(t') e^{\kappa(t-t')/\delta^2} \operatorname{erfc}\left(\frac{\sqrt{\kappa(t-t')}}{\delta}\right) dt', \quad (31)$$

where δ is the e-folding length of the heat source due to the runaways into the PFCs, $\operatorname{erfc}(x) = 1 - \frac{2}{\sqrt{\pi}} \int_0^x e^{-x'^2} dx'$ is the complementary error function, $\kappa = K/\rho c$ (K is the solid heat conductivity, c the heat capacity, and ρ the solid density), $q_r \equiv P_r/A_w$ is the heat flux density, and A_w the runaway wetted area.

This simplified analysis does not include a number of effects which should be considered for a more accurate evaluation of the runaway heat loads such as the runaway distribution function, the ratio of the perpendicular (to the magnetic field) to the parallel runaway energy, or the detailed plasma magnetic configuration and geometry of the PFCs [33, 34, 35].

On the other hand, as in the case of Ref. [10], here we will focus on the effect of the runaway electrons on the ITER Be first wall as "it is expected that the impact of runaways on the Be first wall will provide a more restrictive criterion to assess the requirements to avoid deep melting of the PFCs by runaways in ITER than that of impact on the W divertor baffle" [10].

Fig. 17 shows, using the evaluation for the power deposited by the runaways of Fig. 16, an estimate of the minimum area (A_{min}) for runaway deposition which would avoid melting of the Be first wall PFCs (i.e., $\Delta T < 1000$ K) for a typical penetration depth of MeV runaway electrons in Be, $\delta = 2$ mm. A deconfinement time $\tau_d = 0.1$ ms is assumed when $q_a = 2$ is crossed. For $n_e = 10^{22} \text{ m}^{-3}$ (dashed dotted line), the minimum wetted area is in the range $\sim 2 \text{ m}^2$ when $q_a = 2$ is reached, sharply increasing to $\sim 5 \text{ m}^2$ as a result of the runaway deconfinement. Although low values of τ_d lead to a small conversion of magnetic into runaway kinetic energy, the runaway power loads can still be large due to the short deposition time, leading to the increase of A_{min} . For $n_e = 5 \cdot 10^{22} \text{ m}^{-3}$ (dashed line), A_{min} is reduced to values in the range of tenths of m^2 when $q_a = 2$ is reached, but still increasing to $A_{min} \sim 2 \text{ m}^2$ during runaway deconfinement. Reducing A_{min} to sufficiently low values even during the deconfinement phase would require larger densities, $\sim 10^{23} \text{ m}^{-3}$, as illustrated by the full line in Fig. 17 which shows the results for $n_e = 7.5 \cdot 10^{22} \text{ m}^{-3}$. To define the precise conditions for Be melting avoidance is not

a simple task as it will depend on the expected runaway runaway wetted area, which otherwise will be affected by the large magnetic fluctuations during deconfinement [25], but a large enough density to reduce the energy deposited on the runaways by the time $q_a = 2$ is reached to small enough values (< 10 MJ) will be a necessary condition.

6 CONCLUSIONS

A simple 0-D model which mimics the plasma surrounded by the conducting structures [12], including self-consistently the vertical plasma motion and the generation of runaway electrons, has been used for an evaluation of the runaway electron formation and termination during the disruption, with particular emphasis on its implications for the case of ITER-like disruptions.

Regarding the formation of the runaway beam, it is found that the total plasma current when the plasma hits the wall increases with the ratio of the current quench time to the wall time (τ_{CQ}/τ_w) as the longer the current quench time, the greater the penetration of external magnetic energy through the vacuum vessel, whereas if $\tau_{CQ} \ll \tau_w$ no external magnetic energy penetrates into the plasma and the current at the wall tends to a constant limiting value. Hence, in the case of ITER, with a highly conducting wall, the total plasma current when the plasma touches the wall is always the same and independent of the amount of impurities injected for disruption mitigation, but the runaway current at that time can significantly decrease for a high enough number of impurities. The vertical plasma velocity increases with the ohmic plasma current and, therefore, decreases for large runaway currents. As a result, if a high number of impurities are injected to dissipate the runaway current, the runaway current decreases, the plasma

column is accelerated and the time to reach the wall can be noticeably shortened.

Once the plasma touches the wall, the scraping-off and termination phase of the runaway current occurs. During this phase, the plasma velocity and electric field can substantially increase leading to the deposition of a noticeable amount of energy on the runaway electrons (\sim hundreds of MJ). The effect of injecting a larger amount of impurities is in part counteracted by the increase of the plasma velocity when reducing the runaway current and, thus, the enhancement of the electric field, so that the decrease of the energy deposition on the runaways is smaller than initially expected. An early second impurity injection can reduce somewhat the amount of energy deposited on the runaway electrons, and it is found that larger temperatures of the residual ohmic plasma during scraping-off might be efficient in reducing the power fluxes onto the PFCs.

It is also found that the plasma reaches the $q_a = 2$ limit before the current is fully terminated and that the amount of energy deposited on the runaway electrons by that time can be substantially lower than the estimates for the full scraping-off of the beam. Negligible additional conversion of magnetic into runaway kinetic energy would be expected during the runaway deconfinement following the large magnetic fluctuations after $q_a = 2$ is crossed for characteristic deconfinement times lower than 0.1 ms, which are typical of ideal MHD instabilities.

An assessment of the power loads due to the runaways on the PFCs has also been carried out. Larger amounts of impurities result in a faster beam motion and induced electric fields, which lead to larger power loads although for a shorter timescale so that, as a whole, the total energy deposited by the runaways decreases at larger densities. The evaluation of the power deposited by the runaway electrons allows to get estimates of the minimum wetted area to avoid melting of the Be FW PFCs for typical penetration depths

of MeV runaway electrons in Be, and suggests that large enough densities ($\sim 10^{23} \text{ m}^{-3}$) would be required, assuming that no more conversion of magnetic energy into runaway energy occurs after the limit $q_a = 2$ is reached ($\tau_d < 0.1 \text{ ms}$), leading to very small energy deposition on the runaway population (typically $< 10 \text{ MJ}$).

Finally, it must be taken into account that, here, for simplicity, the effect of the injection of impurities has been just accounted for by increasing the density n_e . Nevertheless, a more accurate treatment taking into account the effect of the collisions with the free and bound electrons, and with the average and the full nuclear charge of the impurity ions, including partial screening effects as in [36], indicates that similar trends are found for the energy deposited on the runaway electrons, ΔW_{run} , as a function of the amount of assimilated impurities and the bulk temperature, T_e . This is illustrated in Fig. 18 which shows the energy deposited on the runaway electrons for an ITER-like 15 MA disruption assuming Ne injection as a function of the amount of assimilated Ne (in $\text{kPa} \cdot \text{m}^3$) (for simplicity only Ne^{1+} is assumed). The squares correspond to the energy deposited assuming that the beam has been fully scraped-off and the circles indicate the energy deposited until the $q_a = 2$ limit is reached. The results assuming $T_e = 3 \text{ eV}$ (full symbols) and $T_e = 5 \text{ eV}$ (open symbols) are compared (of course, this is a simplified approach and a more adequate calculation would require a self-consistent calculation of T_e as well, instead of assumed given values for the bulk plasma temperature, which is beyond the scope of this work). In all the cases a runaway seed current $I_{seed} = 10^{-4} \text{ MA}$ has been assumed. The figure would suggest that in order to avoid Be melting, which would demand a very low amount of energy deposited on the runaways, $\sim 10 \text{ kPa} \cdot \text{m}^3$ of assimilated Ne would be required (assuming that no more conversion of magnetic energy into runaway energy occurs once the limit $q_a = 2$ is reached). Fig. 18 assumes that the

impurities are in the plasma since $t = 0$ s. The effect of a first injection followed by a second injection at a time Δt was discussed in Fig. 8 in Sec. 4, showing that although ΔW_{run} is somewhat reduced by earlier injections, the effect is not sizeable.

ACKNOWLEDGEMENTS

The first autor wishes to thank F.J. Artola for helpful suggestions. This work was done under support from Projects ENE2015-66444-R (MINECO/FEDER, UE) and PID2019-110734RB-I00 (AEI, Spain), from Comunidad de Madrid under the agreement with UC3M in the line of Excellence of University Professors (EPUC3M14) and has been carried out under the coordinated research programme of the Disruption and Runaway Theory and Simulation group of the ITER Scientist Fellow Network to which the first author belongs. ITER is the Nuclear Facility INB no. 174. This paper explores physics processes during the plasma operation of the tokamak when disruptions take place; nevertheless the nuclear operator is not constrained by the results of this paper. The views and opinions expressed herein do not necessarily reflect those of the ITER Organization.

References

- [1] NYGREN, R., et al., J.Nucl.Mater. **241-243** (1997) 522.
- [2] LEHNEN, M., et al., "R&D for reliable disruption mitigation in ITER" Preprint: 2018 IAEA Fusion Energy Conference, Gandhinagar [EX/P7-12]
- [3] MARTIN-SOLIS, J.R., LOARTE, A., and LEHNEN, M., Nucl.Fusion **57** (2017) 066025.
- [4] HENDER, T.C., et al., Progress in the ITER Physics Basis **Chapter 3: MHD stability, operational limits and disruptions** Nucl.Fusion **47** (2007) S128 - S202 (beginning of chapter).
- [5] PUTVINSKI, S., et al., Plasma Phys. Controlled Fusion **39** (1997) B157.
- [6] RIEMANN, J., et al., Phys.Plasmas **19** (2012) 012507.
- [7] KONOVALOV, S., et al., "Assessment of the runaway electron energy dissipation in ITER" Preprint: 2016 IAEA Fusion Energy Conference, Kyoto [TH/7-1]
- [8] LOARTE, A., et al., Nucl.Fusion **51** (2011) 073004.
- [9] HOLLMANN, E., et al., Nucl.Fusion **53** (2013) 083004.
- [10] MARTIN-SOLIS, J.R., et al., Nucl.Fusion **54** (2014) 083027.
- [11] HOLLMANN, E.M., et al., Phys.Plasmas **24** (2017) 062505.
- [12] KIRAMOV, D.I. and BREIZMAN, B.N., Phys.Plasmas **24** (2017) 100702.
- [13] BREIZMAN, B.N., et al., Nucl.Fusion **59** (2019) 083001.

- [14] DREICER, H., Phys.Rev. **117**, (1960) 329.
- [15] CONNOR, J.W. and HASTIE, R.J., Nucl.Fusion **15** (1975) 415.
- [16] SMITH, H. and VERWICHTE, E., Phys.Plasmas **15** (2008) 072502.
- [17] MARTIN-SOLIS, J.R., LOARTE, A. and LEHNEN, M., Phys.Plasmas **22** (2015) 082503.
- [18] ROSENBLUTH, M.N. Rosenbluth and PUTVINSKI, S.V., Nucl.Fusion **37** (1997) 1355.
- [19] JAYAKUMAR, H.H., et al., Phys. Lett. A **172** (1993) 447.
- [20] ALEYNIKOV, P., et al., "Kinetic modelling of runaway electrons and their mitigation in ITER" [TH/P3-38], paper presented at 25th IAEA Int. Conf. on Fusion Energy St Petersburg 2014.
- [21] ZHOGOLEV, V.E. and KONOVALOV, S.V., VANT series Nuclear Fusion **37** (2014) 71.
- [22] MARTIN-SOLIS, J.R., LOARTE, A. and LEHNEN, M., Phys.Plasmas **22** (2015) 092512.
- [23] HESSLOW, L., et al., Phys.Rev.Lett **118** (2017) 255001.
- [24] LEHNEN, M., Private Communication (2018).
- [25] PAZ-SOLDAN, C., et al., Plasma Phys. Controlled Fusion **61** (2019) 054001.
- [26] REUX, C., et al., Phys.Rev.Lett **126** (2021) 175001.

- [27] RECHESTER, A. B. and ROSENBLUTH, M. N., Phys. Rev. Lett. **40** (1978) 38.
- [28] RICCARDO, V. and LOARTE, A., Nucl.Fusion **45** (2005) 1427.
- [29] MARTIN-SOLIS, J.R., Phys.Plasmas **28** (2021) 032505.
- [30] CARSLAW, H.S., JAEGER, J.C., Conduction of Heat in Solids, Oxford Universty Press, London, 1959.
- [31] LEHNEN, M., et al., J.Nucl.Mater. **390-391** (2009) 740.
- [32] VanSANT, J.H., Conduction Heat Transfer Solutions, UCRL-52863, Lawrence Livermore National Lab., 1980.
- [33] MADDALUNO, G., et al., J.Nucl.Mater. **313-316** (2003) 651.
- [34] BAZYLEV, B., et al., J.Nucl.Mater. **415** (2011) S841.
- [35] BAZYLEV, B., et al., J.Nucl.Mater. **438** (2013) S237.
- [36] HESSLOW, L., et al., Nucl. Fusion **59** (2019) 084004.

FIGURE CAPTIONS

Fig. 1 Comparison between the plasma current at the time the plasma column touches wall as a function of τ_{CQ}/τ_w for a 15 MA ITER-like disruption and $n_e = 4 \times 10^{21} \text{ m}^{-3}$ (full line), $n_e = 2.5 \times 10^{20} \text{ m}^{-3}$ (dashed line). A runaway seed $I_{seed} = 0.03 \text{ MA}$ is assumed.

Fig. 2 Plasma current (open dots) and runaway current (full dots) as a function of density for a 15 MA ITER-like disruption ($I_{seed} = 0.03 \text{ MA}$, $T_e = 5 \text{ eV}$, $\tau_w = 0.5 \text{ s}$).

Fig. 3 Vertical plasma velocity as a function of n_e for a 15 MA ITER-like disruption for the same conditions than previous figure.

Fig. 4 For a 15 MA ITER-like disruption ($\tau_w = 0.5 \text{ s}$, $T_e = 5 \text{ eV}$), assuming $I_{seed} = 0.03 \text{ MA}$ and $n_e = 10^{22} \text{ m}^{-3}$: Top: Plasma and runaway currents as a function of time; Bottom: Time evolution of the electric field (full line). The dashed line indicates the effective critical electric field, E_R^{eff} , and the horizontal line corresponds to the avalanche runaway threshold, E_R .

Fig. 5 For the same conditions than previous figure: energy deposited onto the runaway electrons, ΔW_{run} , as a function of time.

Fig. 6 For a 15 MA ITER-like disruption ($\tau_w = 0.5 \text{ s}$, $T_e = 5 \text{ eV}$), assuming $I_{seed} = 0.03 \text{ MA}$ and $n_e = 5 \times 10^{22} \text{ m}^{-3}$: Top: Plasma and runaway currents as a function of time; Bottom: Time evolution of the electric field. The dashed line indicates the effective critical electric field, E_R^{eff} , and the horizontal line corresponds to the avalanche runaway threshold, E_R .

Fig. 7 For the same conditions than previous figure: energy deposited onto the runaway electrons, ΔW_{run} , as a function of time.

Fig. 8 For the same 15 MA disruptions than previous figures: energy deposited on the runaway electrons during the scraping-off phase as a function of density. A density $n_e = 5 \times 10^{21} \text{ m}^{-3}$ is assumed at the start of the CQ increasing to n_e due to a second impurity injection at Δt .

Fig. 9 Time evolution of $q_a = q(r = a)$ during the formation, scraping-off and the termination of the runaway current for the disruption of Fig. 4 ($n_e = 10^{22} \text{ m}^{-3}$). The horizontal dashed line indicates $q_a = 2$.

Fig. 10 Energy deposited on the runaway electrons during the scraping-off phase when $q_a = 2$ is reached as a function of density for the same conditions than previous figures, assuming $\Delta t = 0 \text{ ms}$, $T_e = 5 \text{ eV}$ (open squares) and $T_e = 10 \text{ eV}$ (open circles). For illustration, the results for the energy deposited during scraping-off until the beam is fully terminated (black squares) are also shown.

Fig. 11 Runaway current as a function of the (normalized) vertical displacement, ξ , for the same conditions than previous figure and different values of the density. The first vertical line indicates the start of the scraping-off phase and the second one the $q_a = 2$ limit.

Fig. 12 $I_r/(1 - \xi)$ as a function of the (normalized) vertical displacement, ξ , during scraping-off for the same conditions than previous figures and different values of the density. The vertical line indicates the $q_a = 2$ limit.

Fig. 13 For $n_e = 10^{22} \text{ m}^{-3}$, $T_e = 5 \text{ eV}$, and $\tau_d = 0.25 \text{ ms}$: Top: Time evolution of the plasma current (full line), ohmic current (dashed line) and runaway current (dashed dot line) during deconfinement (after $q_a = 2$ is reached); Bottom: Time evolution of the energy deposited on the runaway electrons during deconfinement.

Fig. 14 For $n_e = 10^{22} \text{ m}^{-3}$, $T_e = 5 \text{ eV}$, and $\tau_d = 0.1 \text{ ms}$: Top: Time evolution of the plasma current (full line), ohmic current (dashed line) and runaway current (dashed dot line) during deconfinement (after $q_a = 2$ is reached); Bottom: Time evolution of the energy deposited on the runaway electrons during deconfinement.

Fig. 15 For the same conditions than Figs. 5 and 7: instantaneous kinetic energy of the runaway beam (dashed lines), W_{kin} , and energy deposited onto the PFCs (full lines), W_{PFC} , as a function of time. The arrows indicate the time at which $q_a = 2$ is reached.

Fig. 16 Runaway power loads onto the PFCs, $P_r(t) \equiv dW_{PFC}/dt$, versus time for the same disruption conditions than previous figure.

Fig. 17 Minimum wetted area to avoid Be melting as function of time for the same disruption conditions than previous figures, for $n_e = 10^{22} \text{ m}^{-3}$ (dash-dotted line), $5 \cdot 10^{22} \text{ m}^{-3}$ (dashed line) and $7.5 \cdot 10^{22} \text{ m}^{-3}$ (full line), including the effect of deconfinement when $q_a = 2$ is reached assuming $\tau_d = 0.1 \text{ ms}$ in all cases. $t = 0$ indicates the start of the scraping-off phase.

Fig. 18 Energy deposited on the runaway electrons for an ITER-like 15 MA disruption assuming Ne injection as a function of the amount of assimilated Ne. A runaway seed current $I_{seed} = 10^{-4} \text{ MA}$ has been assumed. Squares: energy deposited until the beam is

fully scraped-off; Circles: energy deposited until the $q_a = 2$ limit is reached. The results for $T_e = 3\text{ eV}$ (full symbols) and $T_e = 5\text{ eV}$ (open symbols) are compared.

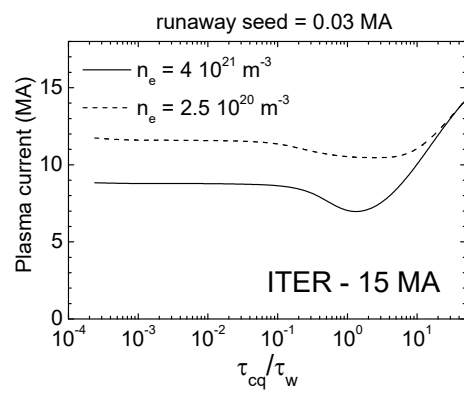


Figure 1:

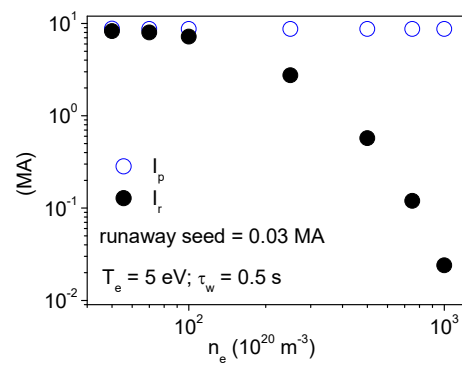


Figure 2:

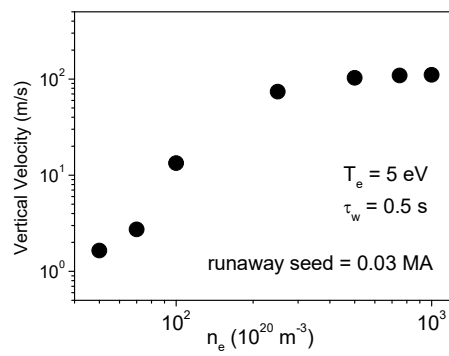


Figure 3:

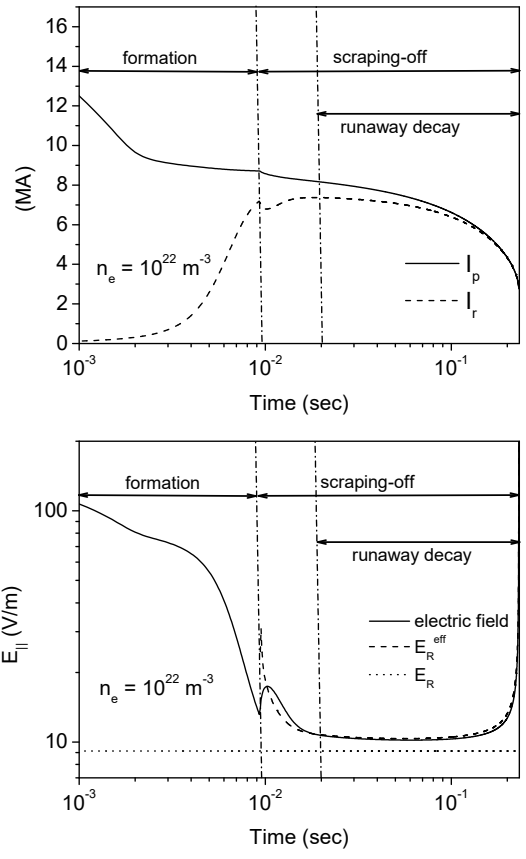


Figure 4:

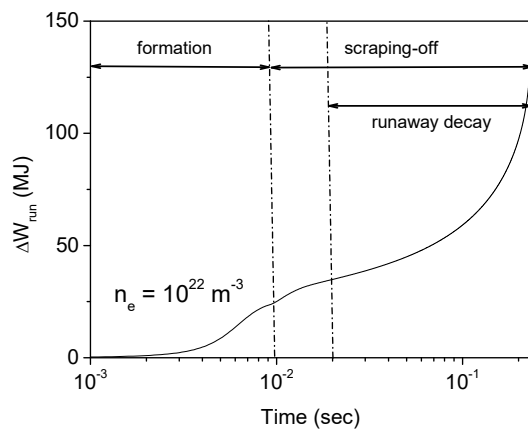


Figure 5:

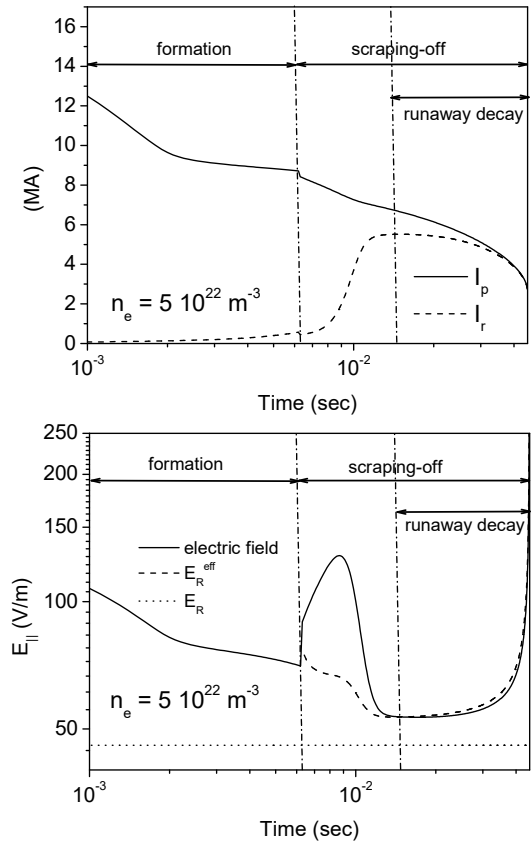


Figure 6:

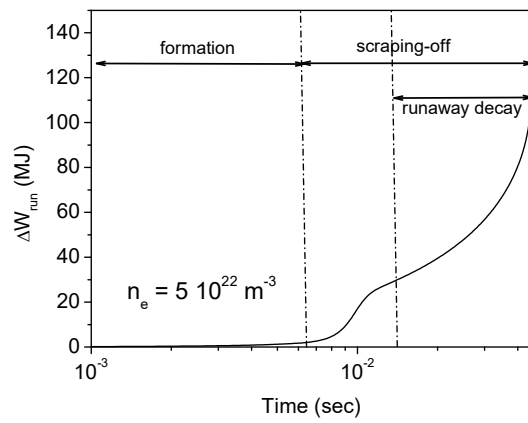


Figure 7:

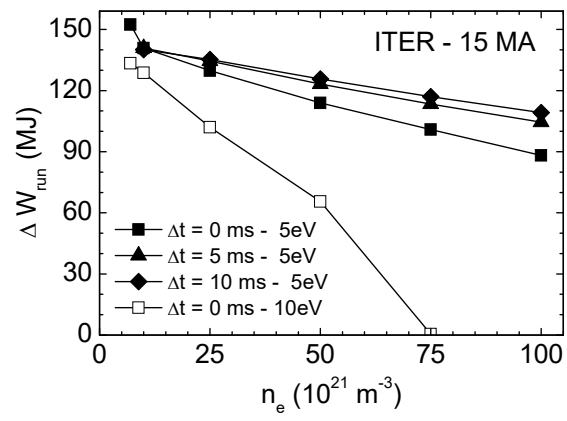


Figure 8:

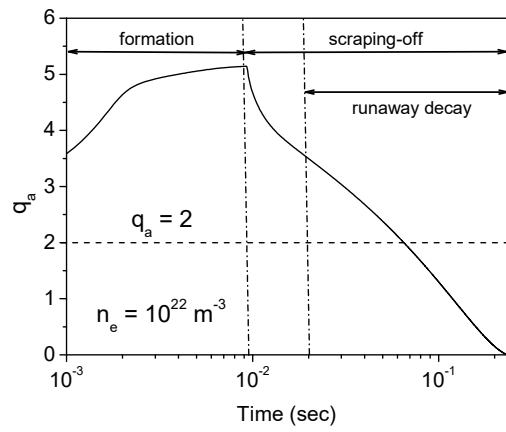


Figure 9:

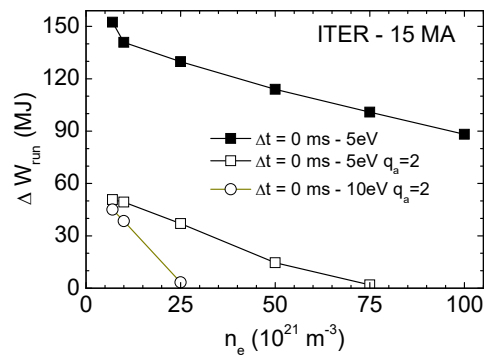


Figure 10:

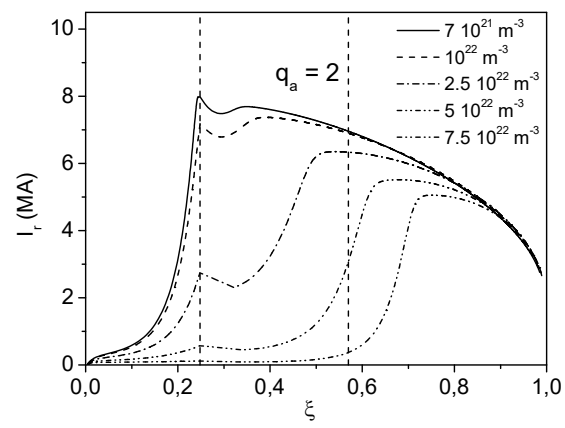


Figure 11:

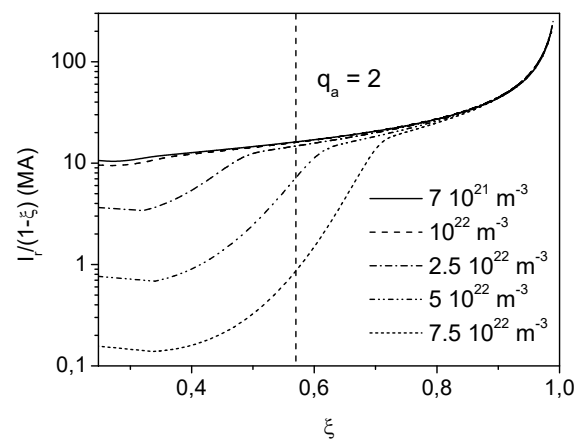


Figure 12:

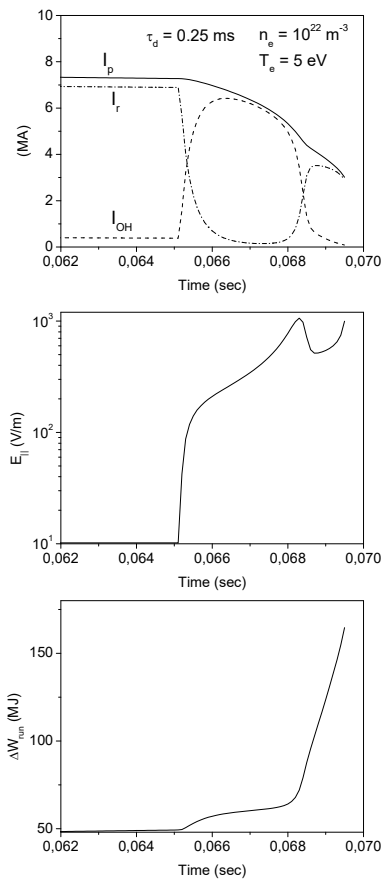


Figure 13:

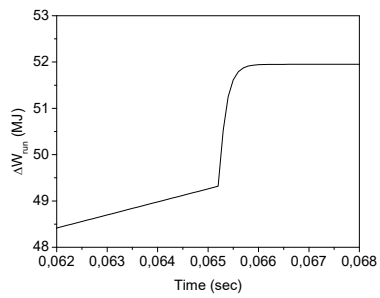
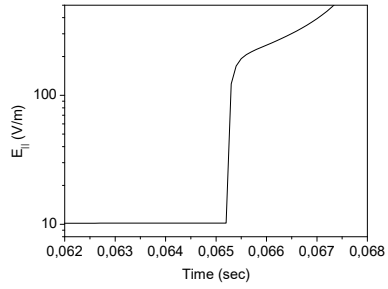
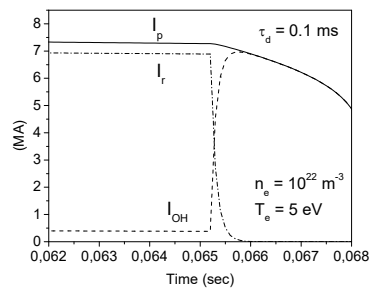


Figure 14:

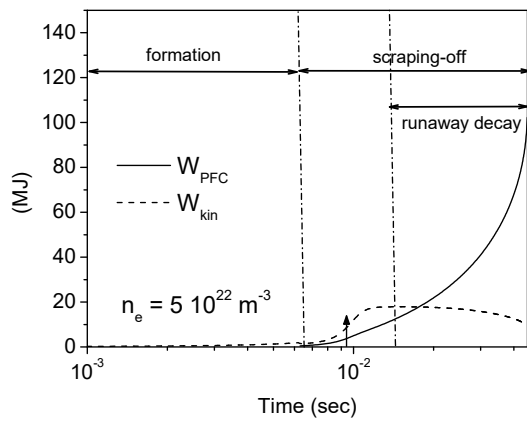
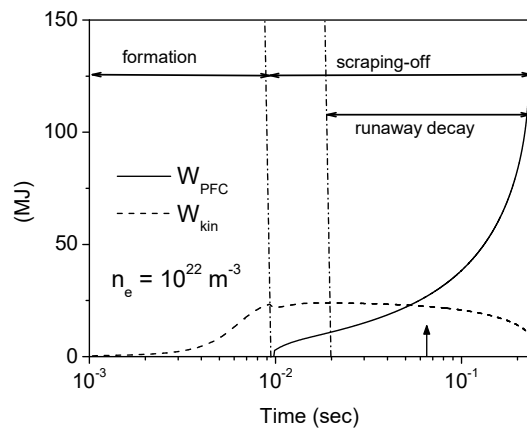


Figure 15:

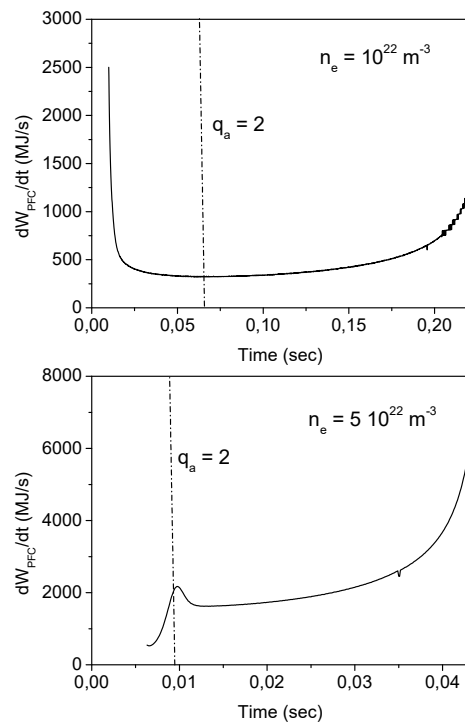


Figure 16:

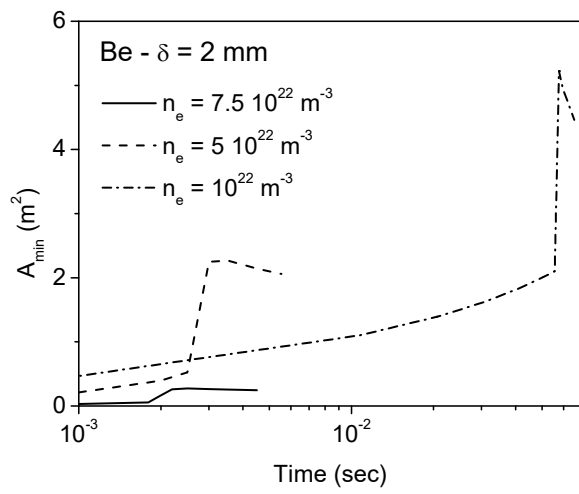


Figure 17:

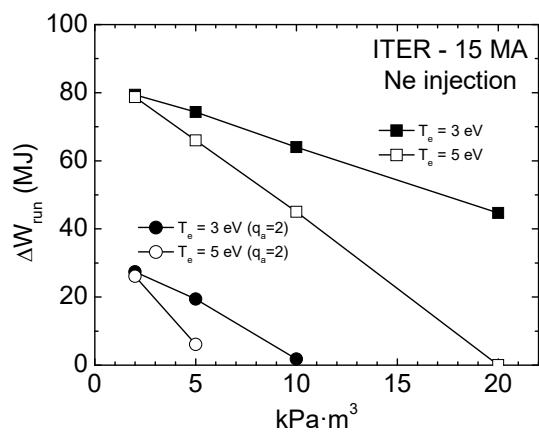


Figure 18: